Supplementary Information (SI) for Journal of Materials Chemistry C.
This journal is © The Royal Society of Chemistry 2024

Reciprocating Thermal Behaviour in a Series of 7-Coordinate Mn(II) and Co(II) Complexes

Le-Shan Zhang,[a,†] Xin-Xin Jin,[b,†] Li-Xin Wang,[a,†] Lu-Lu Liu,[a] Rui-Yue Qi,[a] Xu Zhang,[c] Bing-Wu Wang,[b] Jing Xiang,[a,*] Ji-Yan Liu,[a,*] and Song Gao.[b,d]

[a.] *Key Laboratory of Optoelectronic Chemical Materials and Devices (Ministry of Education), School of Optoelectronic Materials and Technology, Jianghan University, Wuhan, 430056. China. E-mail: xiangjing35991@sohu.com*

[b.] *State Key Laboratory of Rare Earth Materials Chemistry and Applications and PKU-HKU Joint Laboratory on Rare Earth Materials and Bioinorganic Chemistry, Peking University, Beijing 100871, P. R. China. E-mail: wangbw@pku.edu.cn.*

[c.] *College of Chemistry and Environmental Engineering, Yangtze University, Jingzhou 434020, Hubei, P. R. China.*

[d.] *School of Chemistry, Sun Yat-Sen University, Guangzhou, China*

[†] These authors contributed equally.

Table of Contents

	Experimental Section	**S1**
Figure S1	The calculated powder X-ray diffraction patterns (red) and the experimental one (black) of **1**-**4**.	**S2-S3**
Figure S2	IR spectrums of **1**-**4**.	**S3**
Figure S3	A view of supramolecular 2D arrangement of **1** through intermolecular H-bonding and π···π interactions and the closest Mn···Mn separation is 5.866 Å.	**S4**
Figure S4	A view of supramolecular 2D arrangement of **2** through intermolecular H-bonding and π···π interactions and the closest Mn···Mn separation is 5.945 Å.	**S4**
Figure S5	A view of supramolecular 2D arrangement of **3** through intermolecular H-bonding interactions and π···π interactions and the closest Mn···Mn separation is 7.395 Å.	**S5**
Figure S6	A view of supramolecular 2D arrangement of **4** through intermolecular H-bonding and π···π interactions and the closest Co···Co separation is 5.924 Å.	**S5**
Figure S7	The χ_M^{-1} vs. *T* polt and the Curie-Weiss Fit of **1**-**4**.	**S6**
Figure S8	The magnetization data for **1**-**4** collected under various dc fields *M* vs *H*/*T* plots.	**S6**
Figure S9	Temperature dependence of the out-of-phase (χ″) signal of the ac magnetic susceptibility for **1** at 100-630 Hz (a) and 630-10 kHz (b) (Hdc = 4 kOe and Hac = 3 Oe).	**S7**
Figure S10	Temperature dependence of in-phase (χ′) signal of the *ac* magnetic susceptibility for **1** (H_{dc} = 4 kOe and H_{ac} = 3 Oe).	**S7**
Figure S11	Frequency dependence of in-phase (χ′) *ac* magnetic susceptibility for **1** (H_{dc} = 4 kOe and H_{ac} = 3 Oe).	**S7**
Figure S12	Temperature dependence of the out-of-phase (χ″) signal of the ac magnetic susceptibility for **2** at 100-446 Hz (a) and 446-10 kHz (b) (Hdc = 4 kOe and Hac = 3 Oe).	**S8**
Figure S13	Temperature dependence of the in-phase (χ′) signal of the ac magnetic susceptibility for **2** (H_{dc} = 4 kOe and H_{ac} = 3 Oe).	**S8**
Figure S14	Frequency dependence of in-phase (χ′) *ac* magnetic susceptibility for **2** (H_{dc} = 4 kOe and H_{ac} = 3 Oe).	**S8**
Figure S15	Temperature dependence of the out-of-phase (χ″) signal of the ac magnetic susceptibility for **3** (Hdc = 1.5 kOe and Hac = 3 Oe).	**S9**
Figure S16	Temperature dependence of the in-phase (χ′) signal of the ac magnetic susceptibility for **3** (H_{dc} = 1.5 kOe and H_{ac} = 3 Oe).	**S9**
Figure S17	Frequency dependence of the in-phase (χ′) signal of the ac magnetic susceptibility for **3** (H_{dc} = 1.5 kOe and H_{ac} = 3 Oe).	**S9**
Figure S18	Temperature dependence of the out-of-phase (χ″) signal of the ac magnetic susceptibility for **4** (Hdc = 1.5 kOe and Hac = 3 Oe).	**S10**
Figure S19	Temperature dependence of the in-phase (χ′) signal of the ac magnetic susceptibility for **4** (H_{dc} = 1.5 kOe and H_{ac} = 3 Oe).	**S10**
Figure S20	Frequency dependence of the in-phase (χ′) signal of the ac magnetic susceptibility for **4** (H_{dc} = 1.5 kOe and H_{ac} = 3 Oe).	**S10**

Figure S21	(a) Cole–Cole plots of **3** at 2–3.5 K (H_{dc} = 1.5 kOe and H_{ac} = 3 Oe); (b) Cole–Cole plots of **3** at 4–15 K (H_{dc} = 1.5 kOe and H_{ac} = 3 Oe). (c) Cole–Cole plots of **4** at 2.5–4 K (H_{dc} = 1.5 kOe and H_{ac} = 3 Oe). (d) Cole–Cole plots of **4** at 4.5–8 K (H_{dc} = 1.5 kOe and H_{ac} = 3 Oe). Solid lines represent best fits to the experimental data according to the generalized Debye model.	**S11**
Figure S22	The ln(τ) *vs*. 1/*T* plot for and the red line represents the fit to a combination of Raman and direct processes for **1** (a), **2** (b), and **3** (c); (d) The ln(τ) *vs*. 1/*T* plot for **4** and the red line represents the fit to a combination of Raman, Orbach, and QTM processes.	**S11-S12**
Figure S23	The ln(τ) *vs*. 1/*T* plot for **1-4** and the red line represents the fit to a combination of $\tau^{-1} = CT^{n} + AB^{m}T + FT^{-1}$.	**S12**
Figure S24	The ln(τ) *vs*. 1/*T* plot for **4** and the red line represents the fit to a combination of Orbach processes.	**S13**
Table S1	Crystal data and structure refinement details for compounds **1, 2, 3** and **4**.	**S14**
Table S2	Parameters of one-component Debye's model for Mn(II) compound **1**.	**S15**
Table S3	Parameters of one-component Debye's model for Mn(II) compound **2**.	**S16**
Table S4	Parameters of one-component Debye's model for Mn(II) compound **3**.	**S16-S17**
Table S5	Parameters of one-component Debye's model for Co(II) compound **4**.	**S18**

Experimental Section

Materials and physical measurements

IR spectra were obtained as KBr discs using a Nicolet 360 FT-IR spectrophotometer. PXRD were collected using an X-ray diffractometer (Empyream, PANalytical B.V.) with a Cu-K_α radiation source. Elemental analysis was performed using an Elementar Vario EL Analyzer. Variable-temperature magnetic susceptibility, *ac* magnetic susceptibility, and field dependence of magnetization were measured on a Quantum Design MPMS XL-5 SQUID system using powder samples made from the crystal samples. Background corrections were done by experimental measurement on the sample holder. The experimental susceptibilities were corrected for the diamagnetism of the constituent atoms (Pascal's tables).

X-ray crystallography

Crystals suitable for X-ray diffraction analysis were obtained for **1, 2, 3** and **4**. X-ray diffraction data were collected at 100 K on an Oxford CCD or a NONIUS Kappa CCD diffractometer using graphite-monochromated Mo K_α radiation (λ = 0.71073 Å) for **1, 2, 3** and **4** in the ω-scan mode. Absorption corrections were done by the multi-scan method. The structures were resolved by the heavy-atom Patterson method or direct methods and refined by full-matrix least-squares using SHELX-97 and expanded using Fourier techniques. All non-hydrogen atoms were refined anisotropically. H atoms were generated by the program SHELXL-97. The positions of H atoms were calculated based on riding mode with thermal parameters equal to 1.2 times that of the associated C atoms and participated in the calculation of final R-indices. Crystallographic data (excluding structure factors) for the structures in this paper have been deposited with the Cambridge Crystallographic Data Centre. Copies of the data can be obtained free of charge on quoting the depository numbers 2337618-2337621 for these compounds.

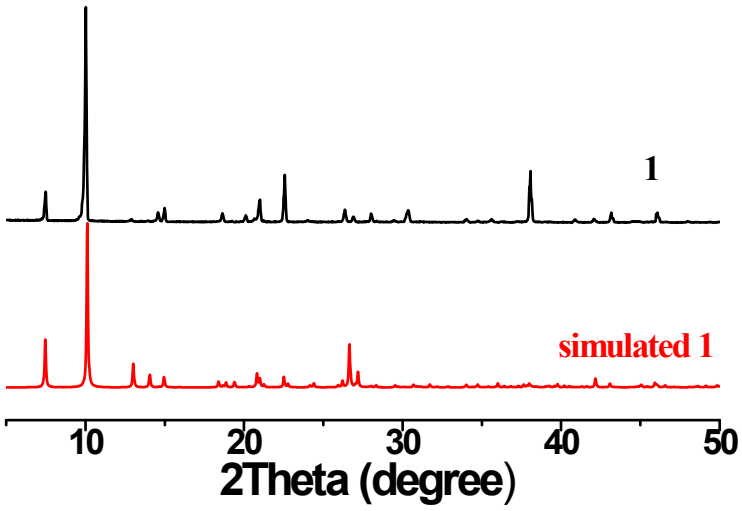
1
simulated 1
10
20
30
40
50
2Theta (degree)

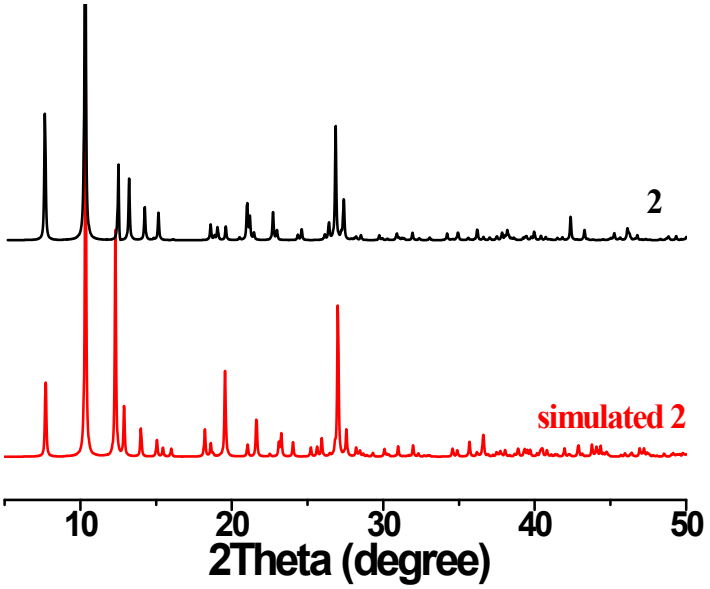
2
simulated 2
10
20
30
40
50
2Theta (degree)

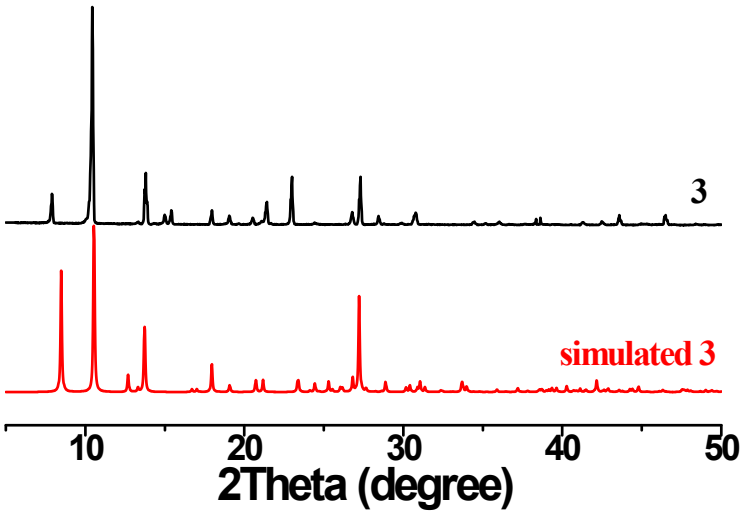
3
simulated 3
10
20
30
40
50
2Theta (degree)

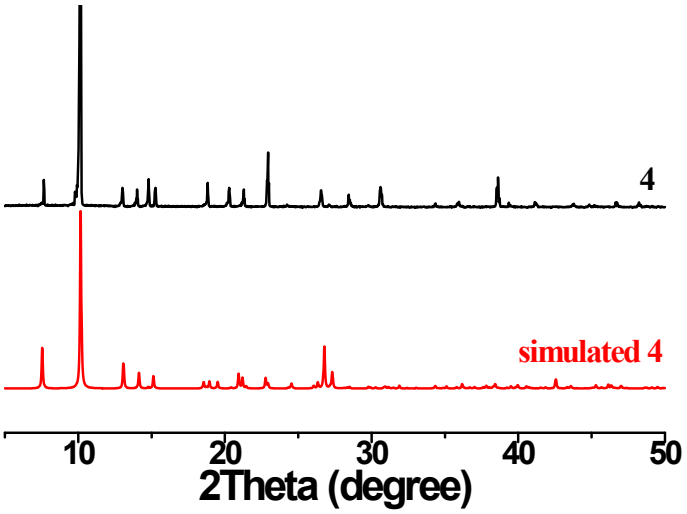

Figure S1. The calculated powder X-ray diffraction patterns (red) and the experimental one (black) of **1-4**.

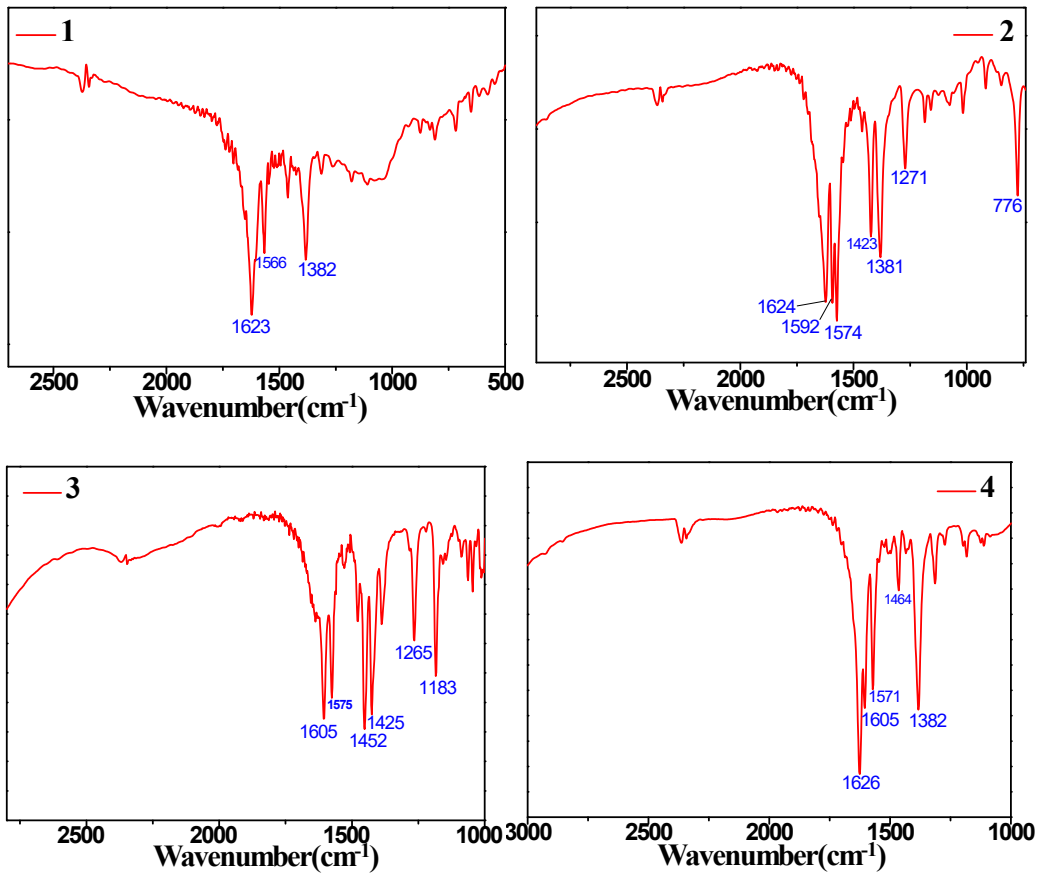

Figure S2. IR spectrums of **1-4**.

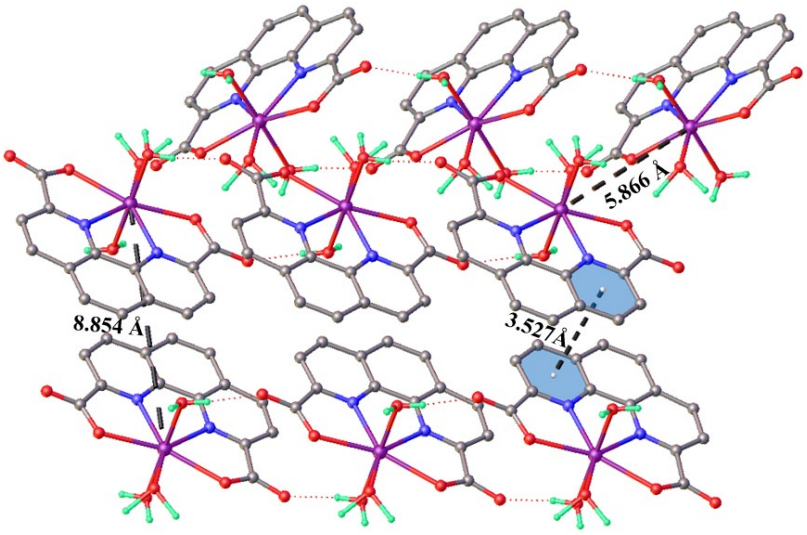

Figure S3. A view of 2D supramolecular network of **1** through intermolecular H-bonding and π···π interactions and the closest Mn···Mn separation is 5.866 Å.

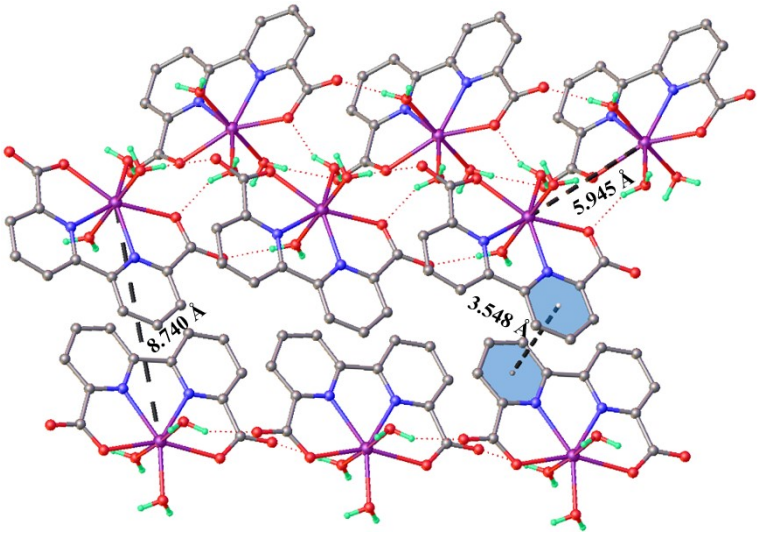

Figure S4. A view of 2D supramolecular network of **2** through intermolecular H-bonding and π···π interactions and the closest Mn···Mn separation is 5.945 Å.

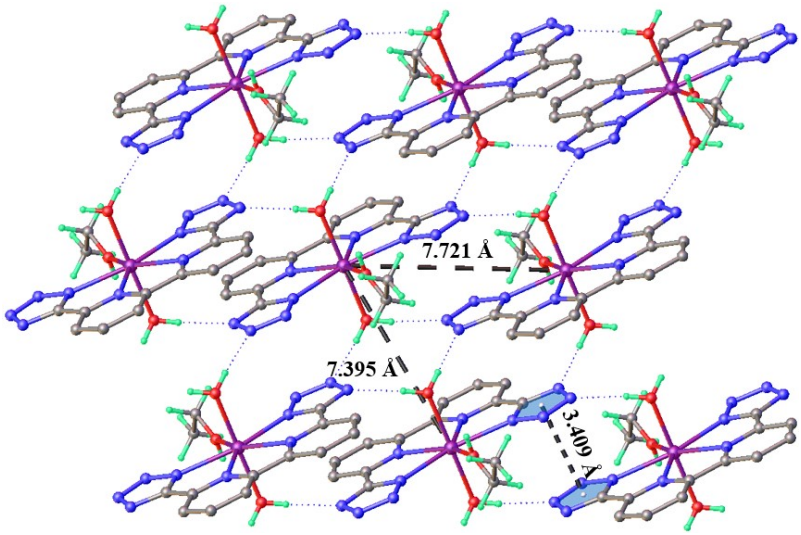

Figure S5. A view of 2D supramolecular network of **3** through intermolecular H-bonding interactions and π···π interactions and the closest Mn···Mn separation is 7.395 Å.

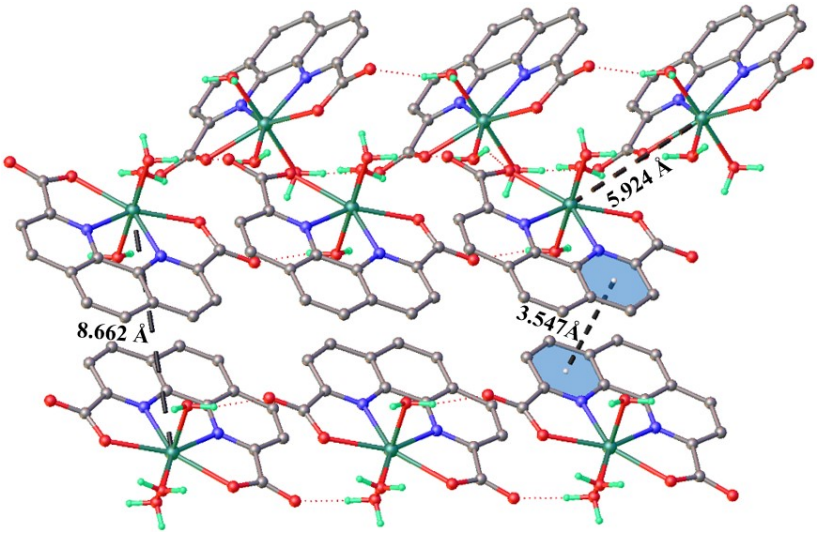

Figure S6. A view of 2D supramolecular network of **4** through intermolecular H-bonding and π···π interactions and the closest Co···Co separation is 5.924 Å.

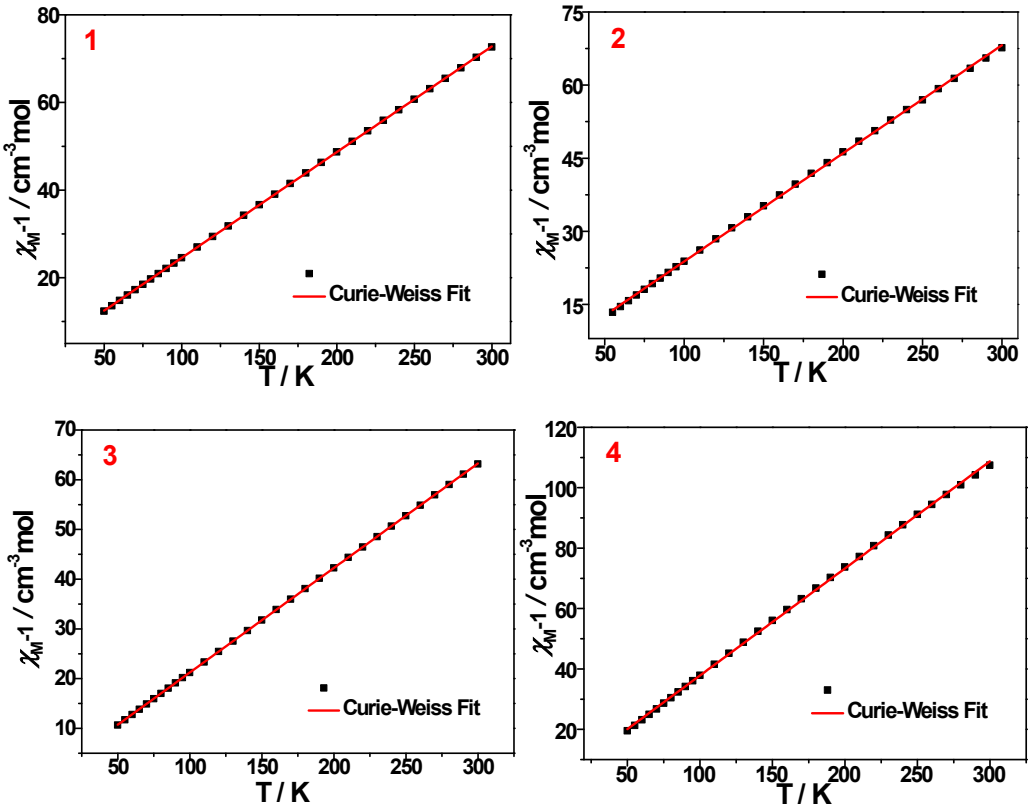

Figure S7. The χ_M^{-1} *vs. T* plot of **1**-**4** and red lines represent the best fit using *Curie-Weiss* law.

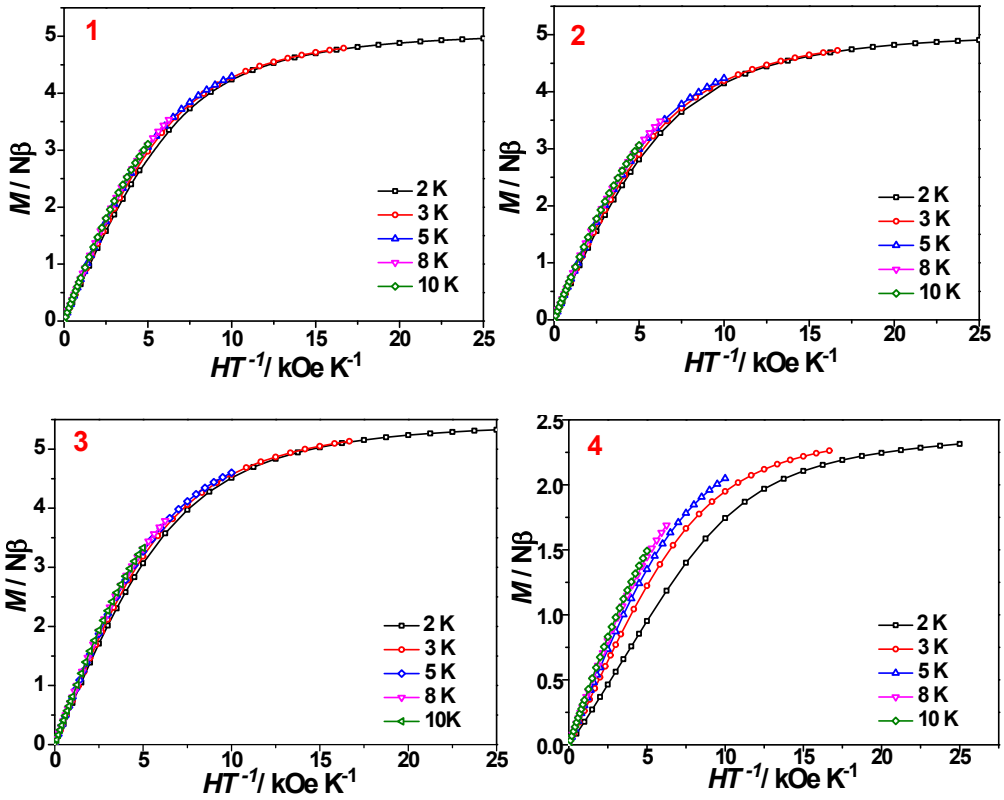

Figure S8. The magnetization data for **1**-**4** collected under various dc fields *M vs. H*/*T* plots.

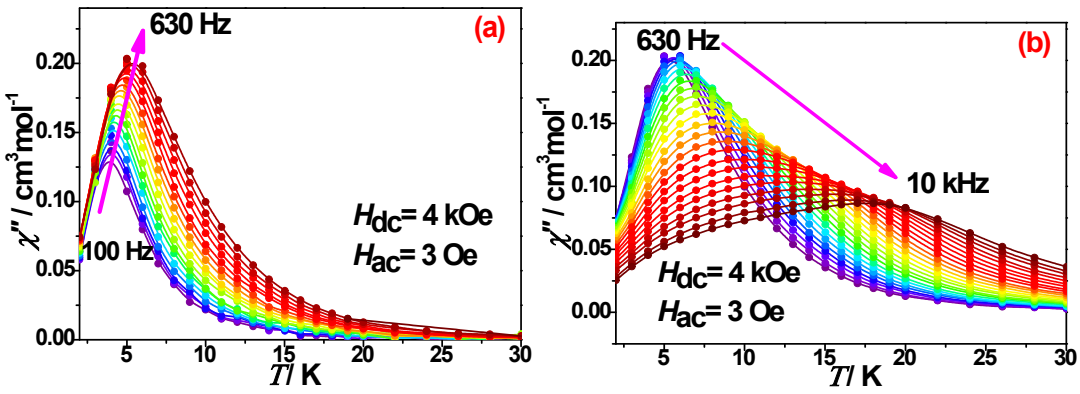

Figure S9. Temperature dependence of the out-of-phase (χ'') signal of the *ac* magnetic susceptibility for **1** at 100-630 Hz (a) and 630-10 kHz (b) (H_{dc} = 4 kOe and H_{ac} = 3 Oe).

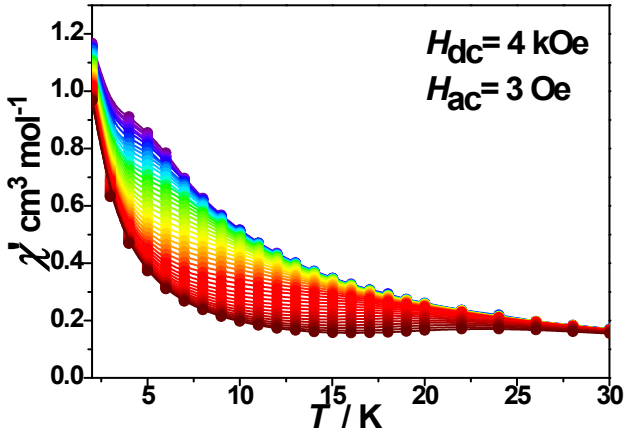

Figure S10. Temperature dependence of in-phase (χ') signal of the *ac* magnetic susceptibility for **1** (H_{dc} = 4 kOe and H_{ac} = 3 Oe).

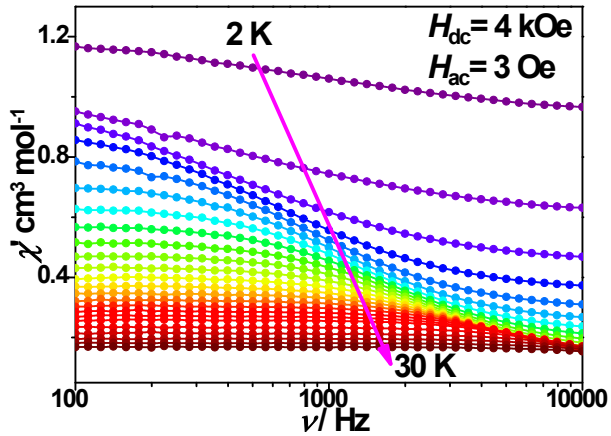

Figure S11. Frequency dependence of in-phase (χ') *ac* magnetic susceptibility for **1** (H_{dc} = 4 kOe and H_{ac} = 3 Oe).

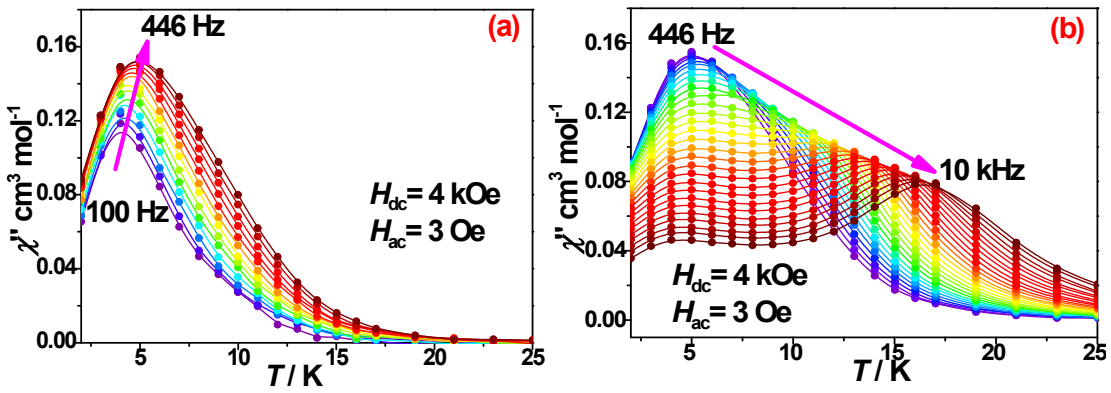

Figure S12. Temperature dependence of the out-of-phase (χ′′) signal of the ac magnetic susceptibility for **2** at 100-446 Hz (a) and 446-10 kHz (b) (H_{dc} = 4 kOe and H_{ac} = 3 Oe).

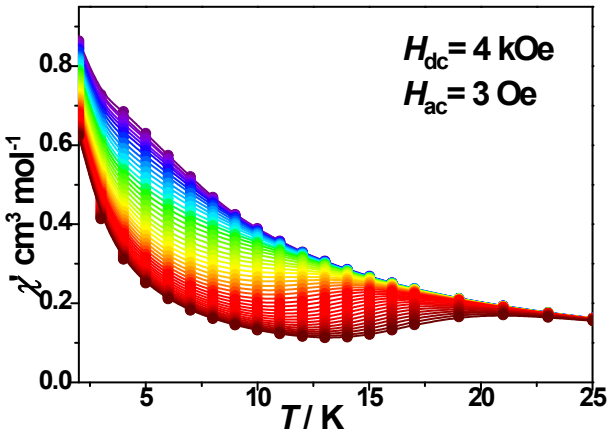

Figure S13. Temperature dependence of the in-phase (χ′) signal of the *ac* magnetic susceptibility for **2** (H_{dc} = 4 kOe and H_{ac} = 3 Oe).

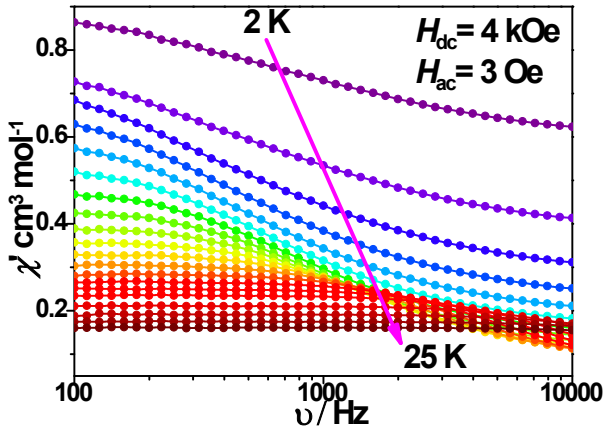

Figure S14. Frequency dependence of in-phase (χ′) *ac* magnetic susceptibility for **2** (H_{dc} = 4 kOe and H_{ac} = 3 Oe).

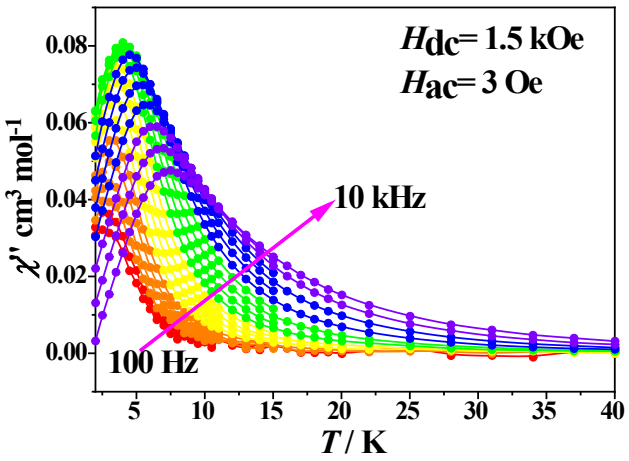

Figure S15. Temperature dependence of the out-of-phase (χ″) signal of the ac magnetic susceptibility for **3** (H_{dc} = 1.5 kOe and H_{ac} = 3 Oe).

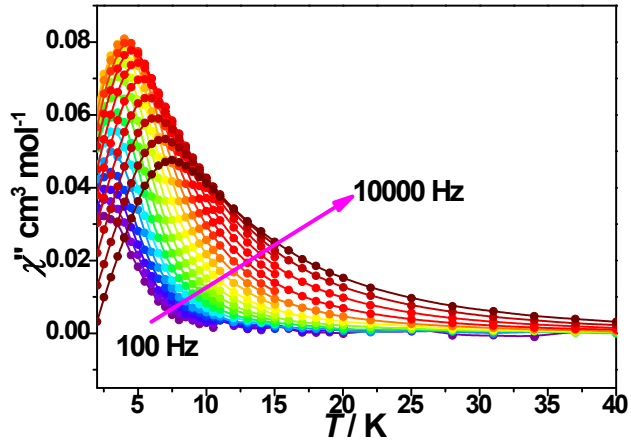

Figure S16. Temperature dependence of the in-phase (χ′) signal of the *ac* magnetic susceptibility for **3** (H_{dc} = 1.5 kOe and H_{ac} = 3 Oe).

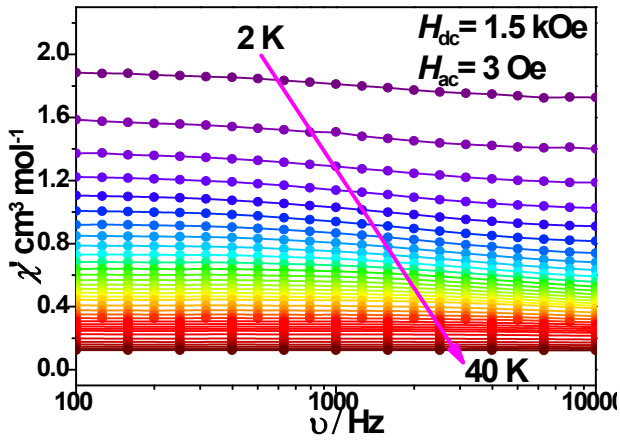

Figure S17. Frequency dependence of the in-phase (χ′) signal of the *ac* magnetic susceptibility for **3** (H_{dc} = 1.5 kOe and H_{ac} = 3 Oe).

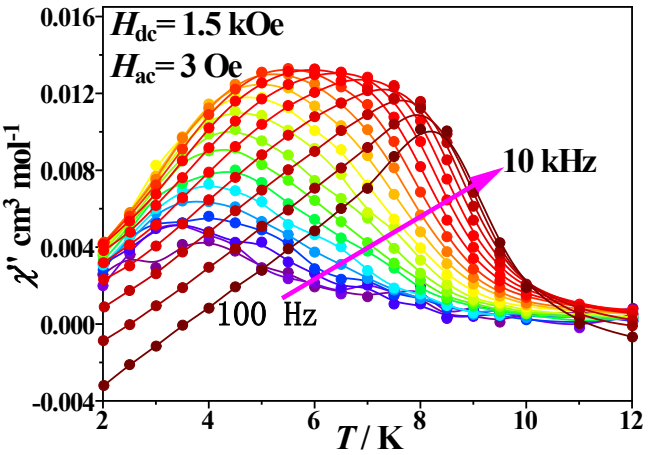

Figure S18. Temperature dependence of the out-of-phase (χ″) signal of the ac magnetic susceptibility for **4** (H_{dc} = 1.5 kOe and H_{ac} = 3 Oe).

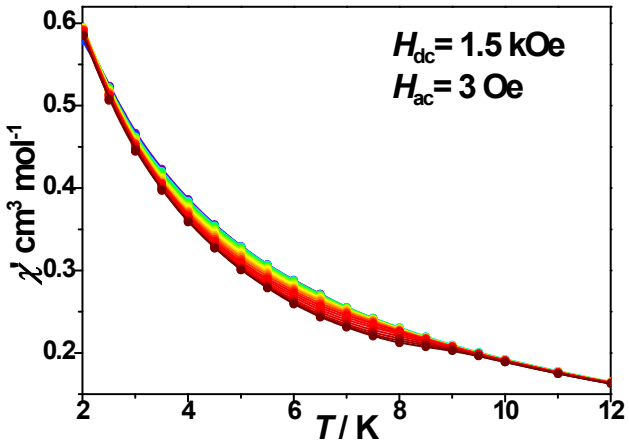

Figure S19. Temperature dependence of the in-phase (χ′) signal of the ac magnetic susceptibility for **4** (H_{dc} = 1.5 kOe and H_{ac} = 3 Oe).

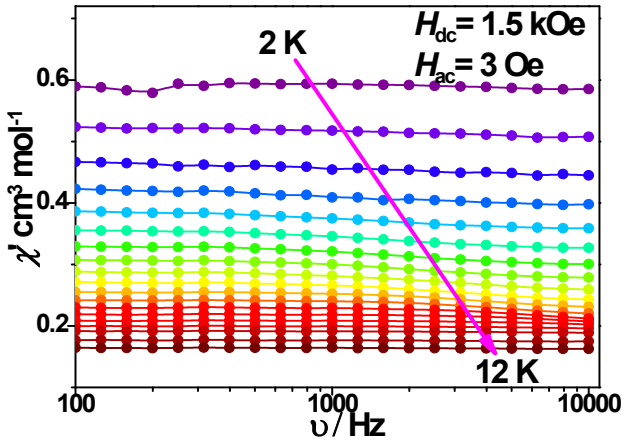

Figure S20. Frequency dependence of the in-phase (χ′) signal of the ac magnetic susceptibility for **4** (H_{dc} = 1.5 kOe and H_{ac} = 3 Oe).

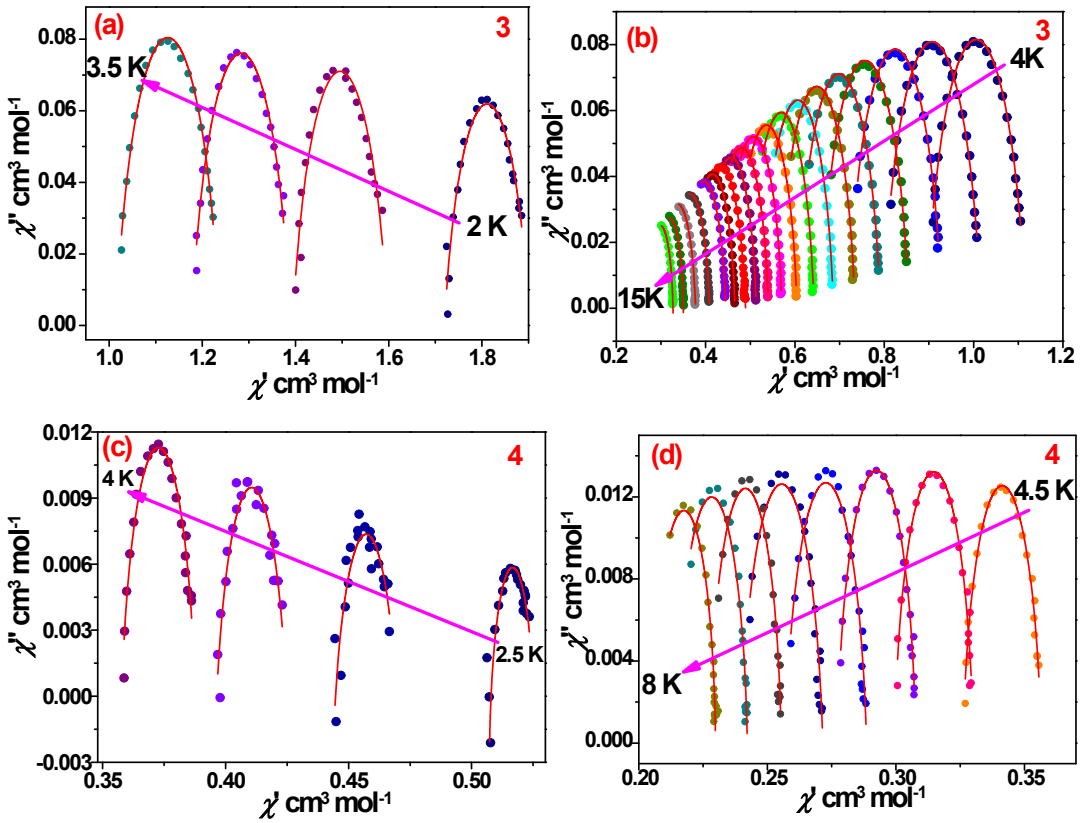

Figure S21. (a) Cole–Cole plots of **3** at 2–3.5 K (H_{dc} = 1.5 kOe and H_{ac} = 3 Oe); (b) Cole–Cole plots of **3** at 4–15 K (H_{dc} = 1.5 kOe and H_{ac} = 3 Oe). (c) Cole–Cole plots of **4** at 2.5–4 K (H_{dc} = 1.5 kOe and H_{ac} = 3 Oe). (d) Cole–Cole plots of **4** at 4.5–8 K (H_{dc} = 1.5 kOe and H_{ac} = 3 Oe). Solid lines represent best fits to the experimental data according to the generalized Debye model.

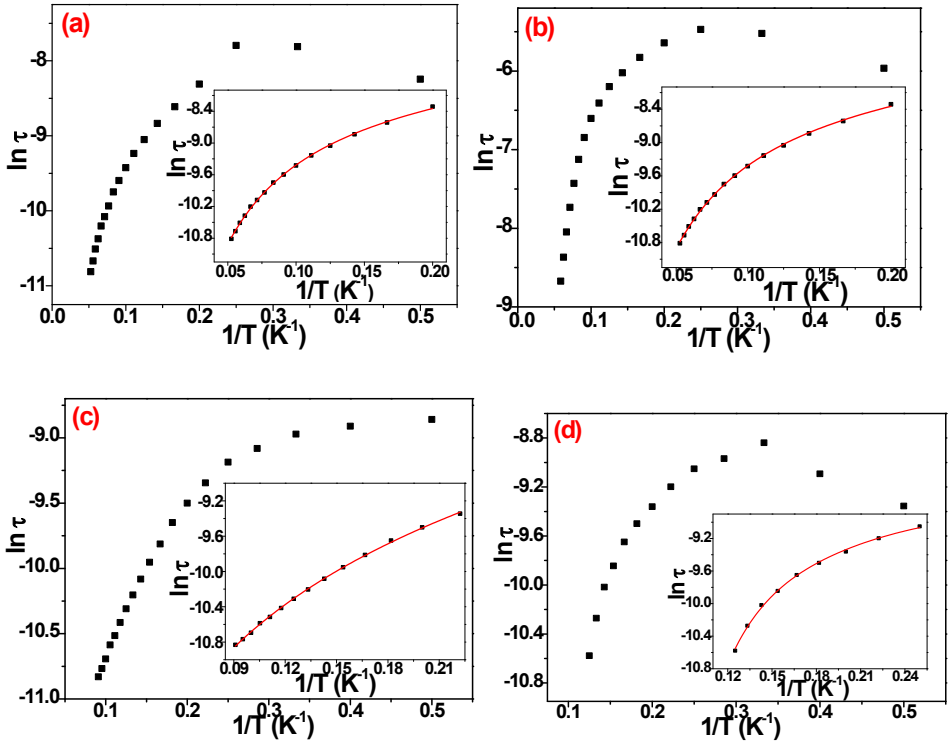

Figure S22. The ln(τ) *vs*. 1/*T* plot and the red line represents the fit to a combination of Raman and direct processes for **1** (a), **2** (b) and **3** (c); (d) The ln(τ) *vs*. 1/*T* plot for **4** and the red line represents the fit to a combination of Raman, Orbach, and QTM processes.

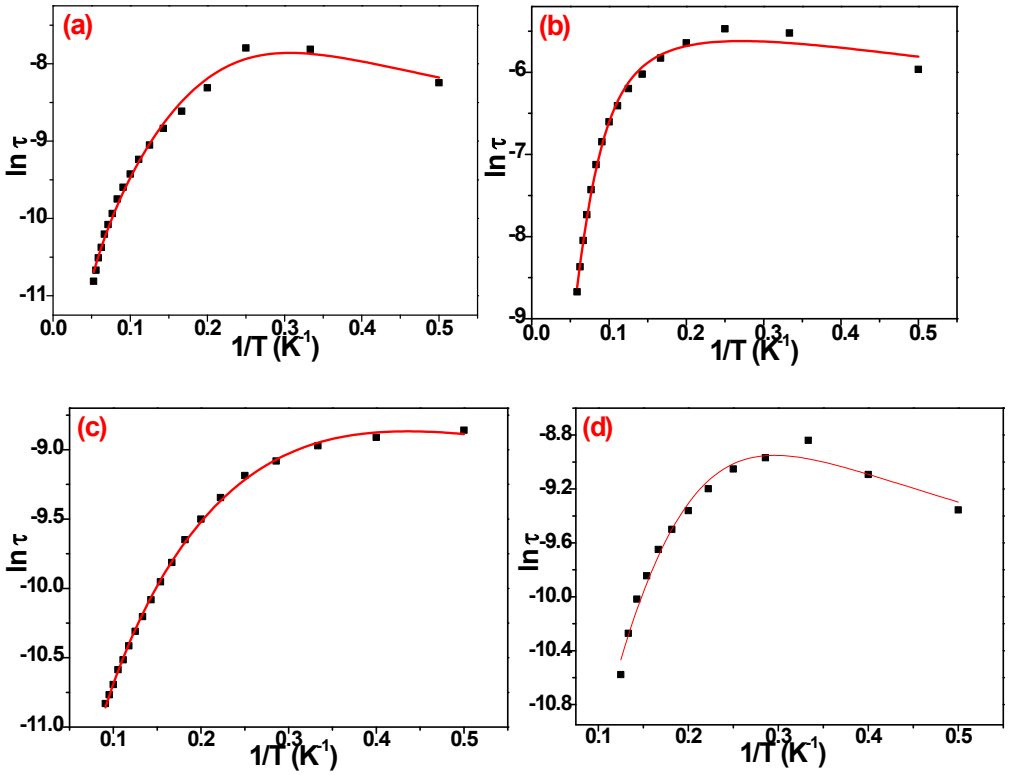

	1(a)	2(b)	3(c)	4(d)
A (s^{-1} K^{-1})	-1738.5	35.7	-1211.1	-709.4
C (s^{-1} K^{-n})	969.48	0.0028	1197.63	171.32
n	1.48	5.07	1.66	0.72
F (K s^{-k})	8650.9	524.5	11744.5	23198.9

Figure S23. The ln(τ) *vs*. 1/*T* plot for **1-4** and the red line represents the fit to a combination of $\tau^{-1} = CT^n + AB^mT + FT^{-1}$.

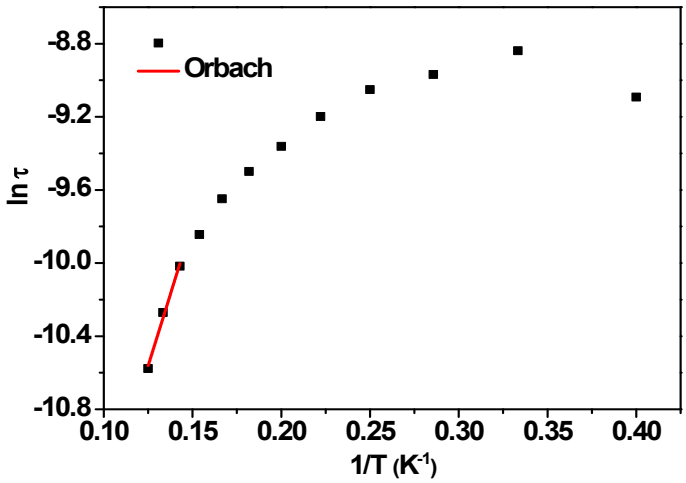

Figure S24. The ln(τ) *vs*. 1/*T* plot for **4** and the red line represents the fit to a combination of Orbach processes.

Table S1. Crystal data and structure refinement details for compounds **1, 2, 3** and **4**.

	1	**2**	**3**	**4**
Formula	$C_{14}H_{12}MnN_2O_7$	$C_{12}H_{12}MnN_2O_7$	$C_{14}H_{16}MnN_{10}O_3$	$C_{14}H_{12}CoN_2O_7$
Mr	375.20	351.17	427.31	379.19
T /K	100	220	100	100
Crystal syst	Orthorhombic	Orthorhombic	Monoclinic	Orthorhombic
Space group	*Fddd*	*Fdd2*	*I2/m*	*Fddd*
a/Å	7.3745 (8)	45.842 (3)	7.3951 (7)	7.3395 (4)
b/Å	18.803 (2)	18.4301 (9)	13.2844 (12)	18.7212 (12)
c/Å	47.340 (4)	7.4950 (4)	16.8246 (19)	46.817 (3)
α, (°)	90	90	90	90
β, (°)	90	90	94.858 (9)	90
γ, (°)	90	90	90	90
V/ Å^3	6564.4 (12)	6332.3 (6)	1646.9 (3)	6432.8 (6)
Z	16	16	4	16
ρ_{calcd}, Mg m^{-3}	1.519	1.662	1.723	1.566
F(000)	3056	3264	876	3088
Collected refl.	11576	8290	4271	7801
Unique refl.	1454	2394	2039	1942
R(int)	0.091	0.054	0.050	0.041
Final *R* indices, *I* > 2σ(I)	R_1(obs)= 0.048 *w*R(all)= 0.105	R_1(obs)= 0.043 *w*R(all)= 0.119	R_1(obs)= 0.063 *w*R(all)= 0.176	R_1(obs)= 0.040 *w*R(all)= 0.103
GOF	1.07	1.09	1.05	1.07
No.of par.	111	228	155	134

Table S2. Parameters of one-component Debye's model for Mn(II) compound **1**.

T / K	χ_S / (cm^3 mol^{-1})	χ_T / (cm^3 mol^{-1})	τ / (s)	α	***Residual***
2.0	0.939546E+00	0.122684E+01	0.253228E-03	0.379905E+00	0.753099E-03
3.0	0.597296E+00	0.108946E+01	0.482289E-03	0.380136E+00	0.830279E-03
4.0	0.437662E+00	0.103222E+01	0.384559E-03	0.291729E+00	0.318679E-03
5.0	0.346850E+00	0.919778E+00	0.254119E-03	0.209224E+00	0.215609E-03

T / K	χ_S / (cm^3 mol^{-1})	χ_T / (cm^3 mol^{-1})	τ / (s)	α	***Residual***
6.0	0.287733E+00	0.810862E+00	0.184944E-03	0.157222E+00	0.277887E-03
7.0	0.246185E+00	0.715791E+00	0.143057E-03	0.126437E+00	0.111200E-03
8.0	0.215093E+00	0.637878E+00	0.114884E-03	0.107670E+00	0.114143E-03
9.0	0.190498E+00	0.575104E+00	0.950867E-04	0.970664E-01	0.872734E-04
10.0	0.170932E+00	0.520034E+00	0.795071E-04	0.873716E-01	0.136497E-03
11.0	0.155591E+00	0.474279E+00	0.677526E-04	0.773725E-01	0.140799E-03
12.0	0.141210E+00	0.435139E+00	0.579818E-04	0.748487E-01	0.891792E-04
13.0	0.129992E+00	0.401195E+00	0.496973E-04	0.679031E-01	0.129354E-03
14.0	0.120963E+00	0.371997E+00	0.429182E-04	0.596959E-01	0.842195E-04
15.0	0.113189E+00	0.347375E+00	0.370758E-04	0.538217E-01	0.684688E-04
16.0	0.106044E+00	0.325040E+00	0.317542E-04	0.461939E-01	0.783867E-04
17.0	0.100126E+00	0.305439E+00	0.273057E-04	0.405787E-01	0.538025E-04
18.0	0.937671E-01	0.287919E+00	0.233797E-04	0.401159E-01	0.785757E-04
19.0	0.892583E-01	0.272096E+00	0.201856E-04	0.344699E-01	0.641940E-04

Table S3. Parameters of one-component Debye's model for Mn(II) compound **2**.

T / K	χ_S / (cm^3 mol^{-1})	χ_T / (cm^3 mol^{-1})	τ / (s)	α	***Residual***
2.0	0.588096E+00	0.933726E+00	0.258442E-03	0.381187E+00	0.224929E-03
3.0	0.373195E+00	0.848330E+00	0.383814E-03	0.388863E+00	0.138465E-03
4.0	0.275522E+00	0.815372E+00	0.417840E-03	0.353797E+00	0.120068E-03

T / K	χ_S / (cm^3 mol^{-1})	χ_T / (cm^3 mol^{-1})	τ / (s)	α	***Residual***
5	0.222935E+00	0.727218E+00	0.349163E-03	0.299102E+00	0.146588E-03
6	0.189585E+00	0.635517E+00	0.283590E-03	0.248619E+00	0.284876E-03
7	0.164726E+00	0.557831E+00	0.232564E-03	0.210030E+00	0.355370E-03
8	0.145807E+00	0.493536E+00	0.191286E-03	0.177488E+00	0.388147E-03
9	0.130061E+00	0.442302E+00	0.156971E-03	0.153617E+00	0.311250E-03
10	0.117702E+00	0.399519E+00	0.127632E-03	0.128783E+00	0.244453E-03
11	0.107033E+00	0.363890E+00	0.101429E-03	0.107316E+00	0.166158E-03
12	0.985596E-01	0.333183E+00	0.784824E-04	0.829755E-01	0.149327E-03
13	0.905063E-01	0.307657E+00	0.592287E-04	0.670896E-01	0.698469E-04
14	0.844338E-01	0.285232E+00	0.438080E-04	0.488596E-01	0.814920E-04
15	0.792264E-01	0.266936E+00	0.324009E-04	0.402235E-01	0.324219E-04
16	0.739828E-01	0.250583E+00	0.238750E-04	0.360787E-01	0.371558E-04

Table S4. Parameters of one-component Debye's model for Mn(II) compound **3**.

T / K	χ_S / (cm^3 mol^{-1})	χ_T / (cm^3 mol^{-1})	τ / (s)	α	***Residual***
2	0.171979E+01	0.190182E+01	0.196029E-03	0.23949E+00	0.772228E-03
2.5	0.139414E+01	0.159800E+01	0.179337E-03	0.22509E+00	0.576992E-03
3	0.117710E+01	0.138908E+01	0.160110E-03	0.20697E+00	0.380630E-03
3.5	0.101465E+01	0.123693E+01	0.141293E-03	0.20238E+00	0.286338E-03

T / K	χ_S / (cm^3 mol^{-1})	χ_T / (cm^3 mol^{-1})	τ / (s)	α	***Residual***
4	0.89535E+00	0.11161E+01	0.121815E-03	0.18985E+00	0.176700E-03
4.5	0.79787E+00	0.10166E+01	0.102035E-03	0.18907E+00	0.110638E-03
5	0.72026E+00	0.92889E+00	0.850794E-04	0.17782E+00	0.615086E-04
5.5	0.65851E+00	0.85506E+00	0.709733E-04	0.16869E+00	0.278212E-04
6	0.60609E+00	0.79138E+00	0.597338E-04	0.16657E+00	0.137410E-04
6.5	0.56370E+00	0.73433E+00	0.514548E-04	0.14972E+00	0.845049E-05
7	0.52665E+00	0.68621E+00	0.446678E-04	0.14725E+00	0.455746E-05
7.5	0.49592E+00	0.64254E+00	0.398236E-04	0.13290E+00	0.806771E-05
8	0.46800E+00	0.60451E+00	0.354796E-04	0.12970E+00	0.720702E-05
8.5	0.44301E+00	0.57066E+00	0.320805E-04	0.12913E+00	0.498706E-05
9	0.42024E+00	0.54071E+00	0.288288E-04	0.13421E+00	0.354293E-05
9.5	0.40041E+00	0.51337E+00	0.264667E-04	0.13251E+00	0.253988E-05
10	0.37690E+00	0.48925E+00	0.223751E-04	0.16554E+00	0.915138E-05
10.5	0.36571E+00	0.46553E+00	0.226490E-04	0.12925E+00	0.329437E-05
11	0.34665E+00	0.44506E+00	0.197980E-04	0.15323E+00	0.785184E-05
12	0.32209E+00	0.40838E+00	0.178661E-04	0.13825E+00	0.300997E-05
13	0.29752E+00	0.37744E+00	0.151813E-04	0.14830E+00	0.559665E-05

14	0.28906E+00	0.35010E+00	0.179656E-04	0.07260E+00	0.460280E-05
15	0.27000E+00	0.32681E+00	0.158262E-04	0.07813E+00	0.500359E-05

Table S5. Parameters of one-component Debye's model for Co(II) compound **4**.

T / K	χ_S / (cm^3 mol^{-1})	χ_T / (cm^3 mol^{-1})	τ / (s)	α	***Residual***
2.5	0.50791E+00	0.52539E+00	0.22953E-03	0.24925E+00	0.288106E-04
3	0.44467E+00	0.46960E+00	0.22111E-03	0.32086E+00	0.338958E-04
3.5	0.39636E+00	0.42478E+00	0.17655E-03	0.25075E+00	0.280189E-04
4	0.35774E+00	0.38769E+00	0.14496E-03	0.17777E+00	0.206576E-04

T / K	χ_S / (cm^3 mol^{-1})	χ_T / (cm^3 mol^{-1})	τ / (s)	α	***Residual***
4.5	0.32598E+00	0.35663E+00	0.12252E-03	0.12658E+00	0.13616E-04
5	0.29943E+00	0.33008E+00	0.10242E-03	0.09359E+00	0.99402E-05
5.5	0.27718E+00	0.30776E+00	0.85965E-04	0.08907E+00	0.72547E-05
6	0.25688E+00	0.28858E+00	0.69392E-04	0.14019E+00	0.11533E-04
6.5	0.23953E+00	0.27153E+00	0.55783E-04	0.14938E+00	0.12134E-04
7	0.22756E+00	0.25536E+00	0.48007E-04	0.07165E+00	0.44199E-05
7.5	0.21439E+00	0.24222E+00	0.34534E-04	0.09415E+00	0.39913E-05
8	0.20519E+00	0.22984E+00	0.25380E-04	0.05298E+00	0.34819E-05